

# Two-fluid model analysis of the terahertz conductivity of YBaCuO samples: optimally doped, underdoped and overdoped cases

Michal Šindler<sup>1</sup>, Wen-Yen Tzeng<sup>2</sup>, Chih-Wei Luo<sup>3-5</sup>, Jiunn-Yuan Lin<sup>5</sup>, and Christelle Kadlec<sup>1</sup>

<sup>1</sup>*Institute of Physics, Academy of Sciences of the Czech Republic,  
Na Slovance 1999/2, 18200 Prague 8, Czech Republic*

<sup>2</sup>*Department of Electronic Engineering, National Formosa University, Yunlin 632, Taiwan*

<sup>3</sup>*Department of Electrophysics, National Yang Ming Chiao Tung University, Hsinchu 30010, Taiwan*

<sup>4</sup>*National Synchrotron Radiation Research Center, Hsinchu, 30076, Taiwan and*

<sup>5</sup>*Institute of Physics, National Yang Ming Chiao Tung University, Hsinchu 30010, Taiwan*

(Dated: October 2, 2023)

The complex conductivity of  $\text{YBa}_2\text{Cu}_3\text{O}_{7-\delta}$  samples representing the optimally doped, the underdoped and the overdoped stoichiometry was measured using time-domain terahertz spectroscopy. In the normal state, the frequency dependence is described by the Drude model. Below the critical temperature  $T_c$ , the two-fluid model was successfully employed to fit all the spectra, from 5 K up to  $T_c$ . The temperature behaviour of fundamental parameters such as the scattering time  $\tau$ , the superfluid fraction  $f_s$  and the conductivity  $\sigma$  was investigated at given frequencies. The real part of the conductivity  $\sigma_1(T)$  exhibits a coherence-like peak at low frequencies, which slightly shifts with increasing frequency whereas its height decreases. It can be observed for all three stoichiometries and its exact shape depends on the quality of the sample. A further analysis shows that this peak is a consequence of the competition between the scattering time  $\tau(T)$  and the superfluid fraction  $f_s(T)$ . The decrease of the superfluid fraction towards  $T_c$  depends on the reduced temperature with a power law close to 2, suggesting a dirty d-wave superconductor case for all levels of doping.

PACS numbers: 74.25.N-, 74.25.Gz

## I. INTRODUCTION

The most studied high-temperature superconductor is undoubtedly  $\text{YBa}_2\text{Cu}_3\text{O}_{7-\delta}$  (YBCO). The exact stoichiometry of oxygen together with its crystal structure is crucial as it determines the hole doping  $p$  and it governs the properties of YBCO. Depending on the hole doping  $p$ , YBCO can transform from an antiferromagnetic compound into a superconductor [1]. Here, we concentrate on the superconducting dome by studying three different cases: an optimally doped sample with the highest possible  $T_c$ , an underdoped sample in which oxygen content is less than in optimally doped samples and finally, an overdoped sample with the highest concentration of oxygen. In order to achieve the overdoped case, the chemical composition was changed by partially replacing Y by Ca resulting in  $\text{Y}_{0.7}\text{Ca}_{0.3}\text{Ba}_2\text{Cu}_3\text{O}_{7-\delta}$  (YCBCO).

Time-domain terahertz spectroscopy allows us to study the temperature dependence of the penetration depth, which is linked to the symmetry of the superconducting order, and of the quasiparticle behaviour, which results in a peak in the real part of the conductivity  $\sigma_1$ . Furthermore, since YBCO is not a regular metal, it is interesting to investigate its behaviour in the normal state as it deviates from the standard behaviour typical of classical metals.

YBCO samples were indeed investigated previously [2–6], but the specificity of our work resides in the comparison of the three types of stoichiometries of films deposited on the same substrate (MgO).

## II. THEORETICAL DESCRIPTION

As currently, there is no universally accepted microscopic theoretical description of high-temperature superconductors, we use the phenomenological description by the two-fluid model.

$$\sigma(\omega) = f_s \frac{ne^2}{m} \left( \pi\delta(\omega) + i\frac{1}{\omega} \right) + (1 - f_s) \frac{ne^2\tau}{m} \frac{1}{1 - i\omega\tau}, \quad (1)$$

where  $f_s$  is the volume fraction of the superfluid fraction,  $n$  is the electron concentration,  $e$  is the elementary charge,  $1/\tau$  is the scattering rate,  $m$  is the effective electron mass,  $\delta(\omega)$  is  $\delta$ -function and  $\omega$  is the circular frequency related to the frequency  $\nu$  by the relation  $\omega = 2\pi\nu$ . While it is customary to refer to frequency  $\nu$  in the experiment, in the theory  $\omega$  is used. The term proportional to  $f_s$  is the London description of the complex conductivity and the other term proportional to  $(1 - f_s)$  describes the normal fluid by using the Drude model. In the DC limit, the normal-state resistivity is  $\rho = 1/\sigma = m/(ne^2\tau)$  thus the temperature dependence of the DC resistivity is driven by the temperature behaviour of the scattering rate.

The superfluid response allows us to determine the London penetration depth  $\lambda$ :

$$\lambda^2 = \frac{1}{\mu_0\sigma_2\omega} = \frac{m}{\mu_0 f_s n e^2}, \quad (2)$$

where  $\mu_0$  is the permeability of vacuum. The penetration depth is related to the pairing mechanism. For clas-

sical superconductors, its temperature dependence is described by the BCS theory [7]. In the case of the d-wave pairing which is more appropriate for cuprates, theories predict a linear temperature dependence of the penetration depth, at least in the  $T \rightarrow 0$  limit [8]. A quadratic dependence can be obtained for d-wave superconductors with strong impurity scattering [9]. Phenomenologically, a temperature dependence  $1 - (T/T_c)^4$  was suggested by Gorter and Casimir [10]. In order to distinguish relevant cases, we use the temperature dependence of the penetration depth by the formula [11]

$$\left[ \frac{\lambda_0}{\lambda(T)} \right]^2 = 1 - \left( \frac{T}{T_c} \right)^\alpha = f_s(T), \quad (3)$$

where  $\lambda_0$  is a standard notation for the London penetration depth in the zero temperature limit and the formula includes all mentioned cases for exponent  $\alpha$  equal to 1, 2 and 4.

### III. EXPERIMENT

#### A. Sample preparation

The  $\text{YBa}_2\text{Cu}_3\text{O}_{7-\delta}$  (YBCO) and  $\text{Y}_{0.7}\text{Ca}_{0.3}\text{Ba}_2\text{Cu}_3\text{O}_{7-\delta}$  (YCBCO) samples used in this study were prepared by pulsed laser deposition (PLD). PLD has an overwhelming superiority over other deposition methods in high- $T_c$  superconducting thin films, since it can rapidly produce high-quality samples. Indeed, YBCO thin films previously used to study optical and time-resolved spectroscopies were often prepared by the PLD method [12–16]. The 248 nm KrF excimer laser was operated at a 5 Hz repetition rate with an energy density of 3 J/cm<sup>2</sup>. The laser beam, with a pulse duration of 25 ns, was focused onto the target surface through a lens, resulting in a spot size of 1 mm  $\times$  3 mm. The laser beam vaporized the YBCO or YCBCO targets, which were then deposited onto a one side polished 10  $\times$  10  $\times$  1 mm<sup>3</sup>-sized (100) MgO substrates at 750 °C with oxygen pressure of 0.3 Torr. The thickness of the YBCO or YCBCO thin films  $d_f$  was controlled to be approximately between 110 and 140 nanometers according to the estimation by excimer laser repetition rates multiplied by the deposition duration and confirmed by scanning electron microscopy (SEM, JEOL JSM7001F). After the PLD, the underdoped YBCO thin film was prepared by post-annealing at 450°C with oxygen pressure of 6 Torr, and the overdoped YCBCO thin film was prepared by post-annealing at 450 °C with oxygen pressure of 10 Torr. All the thin films were first characterized by X-ray diffraction (XRD, BrukerD8) for information about the crystallinity and impurities. The results indicate that all the samples are pure c-axis-oriented YBCO or YCBCO.

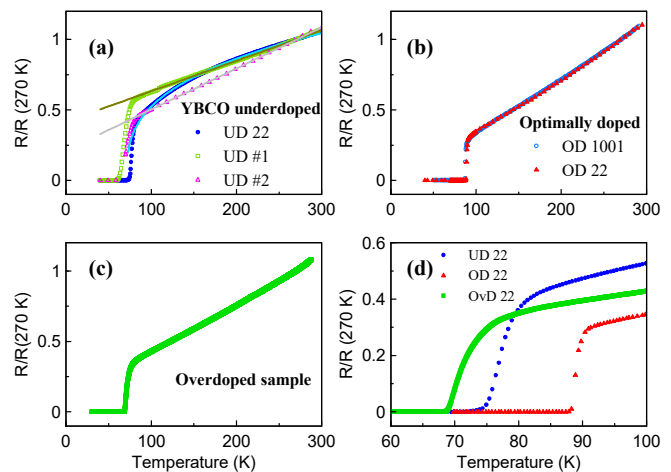


FIG. 1. Temperature dependence of the resistivity for underdoped samples (panel a), optimally doped samples (panel b) and overdoped sample (panel c). Details of the resistivity around the transition are given for three selected samples in panel (d).

#### B. DC resistivity

The transport measurements were applied to determine the superconductivity and transition temperatures of the films. The temperature-dependent resistivities  $R(T)$  (Fig. 1) were measured by the standard four-probe configuration in physical properties measurement systems (PPMS, Quantum design PPMS). The sharp transition to the superconducting state suggests the high quality of the samples. The critical temperatures  $T_c$  reported here were determined as an average value of the temperature where the resistance starts to drop and the temperature where resistivity reaches zero. The critical temperatures and the hole dopings of the samples are listed in Table I, where UD stands for underdoped, OD for optimally doped and OvD for overdoped sample.

In all but one measurement, the DC resistivity in the normal state is very well described by a linear dependence. The optimally doped sample OD 22 exhibits a nearly identical resistivity dependence as the sample prepared previously [13], even though the latter was grown on LAO and OD 22 on MgO. For the underdoped sample, we observed that the resistivity deviates from the linear behaviour. Phenomenologically, we found that  $R(T)$  is proportional to  $(T - T_c)^{1/3}$ .

It is possible to determine the hole doping from the critical temperature. Presland [17] reported that in various high- $T_c$  superconductors or various stoichiometries, the hole doping can be determined from the parabolic relation  $T_c/T_c(\text{max}) = 1 - 82.6(p - 0.16)^2$ , where  $p$  is the number of holes per Cu and  $T_c(\text{max})$  is the maximal critical temperature for the optimal doping. In our case, it is  $T_c(\text{max})=92$  K for all YBaCuO samples and  $T_c(\text{max})=85$  K for the sample with Ca atoms. However, Liang [18] observed deviations from this formula

in YBCO samples and proposed a corrected dependence of the hole doping on  $T_c$ . Here, we denote the corrected hole doping as  $p^*$ .

TABLE I. Resistivity measurements:

Sample	$d_f$ (nm)	$T_c$ (K)	$p$	$p^*$
UD #1	70	70	.106	.128
UD #2	100	70	.106	.128
UD 22	140	77.5	.116	.135
OD 1001 [13]	107	88	.137	.146
OD 21	250	89	.140	.147
OD 22	140	89	.140	.147
OvD 22	110	72	.203	.203

### C. Terahertz spectroscopy

The experiments were performed using a custom-made THz time-domain spectrometer powered with a Ti:sapphire femtosecond laser oscillator (Coherent, Mira). For the generation of linearly polarized THz pulses we used a biased-semiconductor emitter (TeraSED, GigaOptics); for their detection, we applied the usual electro-optic sampling scheme [19] with a 1 mm thick  $\langle 110 \rangle$  ZnTe crystal. The measurements were realized in the transmission geometry under normal incidence in a helium flow cryostat (Optistat, Oxford Instruments).

The frequency ( $\nu$ ) dependence of the complex transmittance  $\tilde{t}(\nu)$  was evaluated as the ratio between the Fourier transforms  $E_s(\nu)$  and  $E_r(\nu)$  of the time profiles transmitted through the sample (film on MgO substrate) and a bare MgO reference of a similar thickness.

A preliminary measurement consists in determining, using the echoes arising from internal reflections in the time profiles, the thickness  $d_{\text{ref}}$  and the complex refractive index  $\tilde{n}_{\text{sub}}(\nu)$  of the reference, which is also that of the substrate. The complex conductivity  $\tilde{\sigma}(\nu)$  of the film can then be calculated from [20]:

$$\tilde{t}(\nu) = \frac{E_s(\nu)}{E_r(\nu)} = \frac{[1 + \tilde{n}_{\text{sub}}(\nu)] e^{i\psi(\nu)}}{1 + \tilde{n}_{\text{sub}}(\nu) + Z_0 \tilde{\sigma}(\nu) d_f}, \quad (4)$$

where  $Z_0$  denotes the vacuum impedance, and  $\psi(\nu)$  is the phase delay due to different optical thicknesses of the sample and the reference. Since the same material is used for the substrate and the reference, we can write

$$\psi(\nu) = \frac{2\pi\nu}{c} [(\tilde{n}(\nu) - 1)d_f + \tilde{n}_{\text{sub}}(\nu)(d_{\text{sub}} - d_{\text{ref}})], \quad (5)$$

where  $c$  is the light velocity,  $\tilde{n}$  is the complex refractive index of the film, and  $d_{\text{sub}}$  is the thickness of the film-supporting substrate.

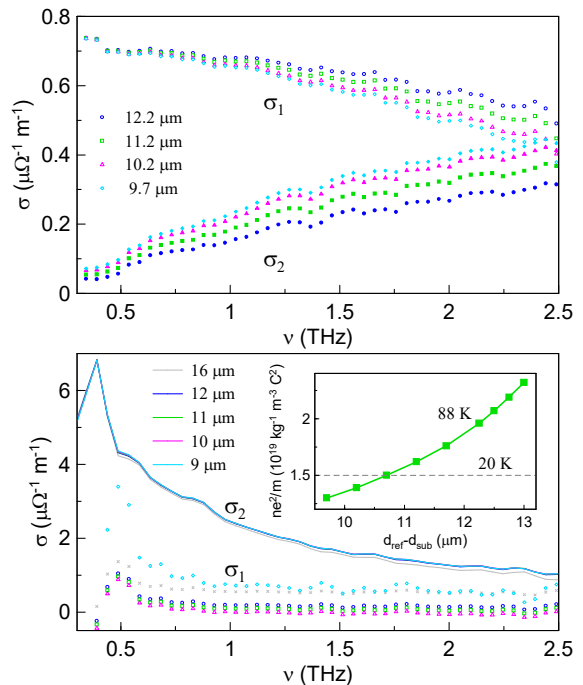


FIG. 2. Complex conductivity  $\tilde{\sigma}(\nu)$  of the optimally doped sample OD 21 in the normal state at 88 K (upper panel) and in the superconducting state at 20 K (bottom panel) evaluated for various thickness differences ( $d_{\text{ref}} - d_{\text{sub}}$ ). In the inset, we compare values of  $ne^2/m$  determined at 20 K and at 88 K for different thickness differences.

The complex conductivity of the film  $\tilde{\sigma}(\nu)$  is linked to its refractive index via the permittivity by the relationships  $\tilde{\epsilon}(\nu) = \tilde{n}(\nu)^2$  and  $\tilde{\sigma}(\nu) = -2\pi i\nu\epsilon_0\tilde{\epsilon}(\nu)$ , where  $\epsilon_0$  denotes the vacuum permittivity.

The accuracy of the measurement of the complex conductivity is determined by the plan-parallelity of the MgO slabs, both the reference and the film-supporting one. The phase measurement is particularly sensitive, as even a small error in the thickness difference ( $d_{\text{sub}} - d_{\text{ref}}$ ) may cause large errors in the determination of the conductivity. For that reason, we used several steps to calculate it.

At low temperatures, the imaginary part of the conductivity  $\sigma_2(\nu)$  is rather insensitive to the phase determination. On the other hand, the real part of the conductivity  $\sigma_1(\nu)$  is quite sensitive to it and could lead to false positive non-zero  $\sigma_1(\nu)$ . This might be a reason for some observations of non-zero  $(1 - f_s)$  at low temperatures in previous studies. So first, we evaluated the complex conductivity of each sample at the lowest temperature and at a temperature slightly above  $T_c$  for various phase shifts obtained by varying the thickness difference ( $d_{\text{ref}} - d_{\text{sub}}$ ). Then we checked that for the optimal thickness difference, the quantity  $ne^2/m$  determined from  $\sigma_2(\nu)$  at low temperature corresponds to the normal state value determined from  $\tilde{\sigma}(\nu)$  just above  $T_c$ . Figure 2 presents the results for the optimally doped sample OD 21. In that

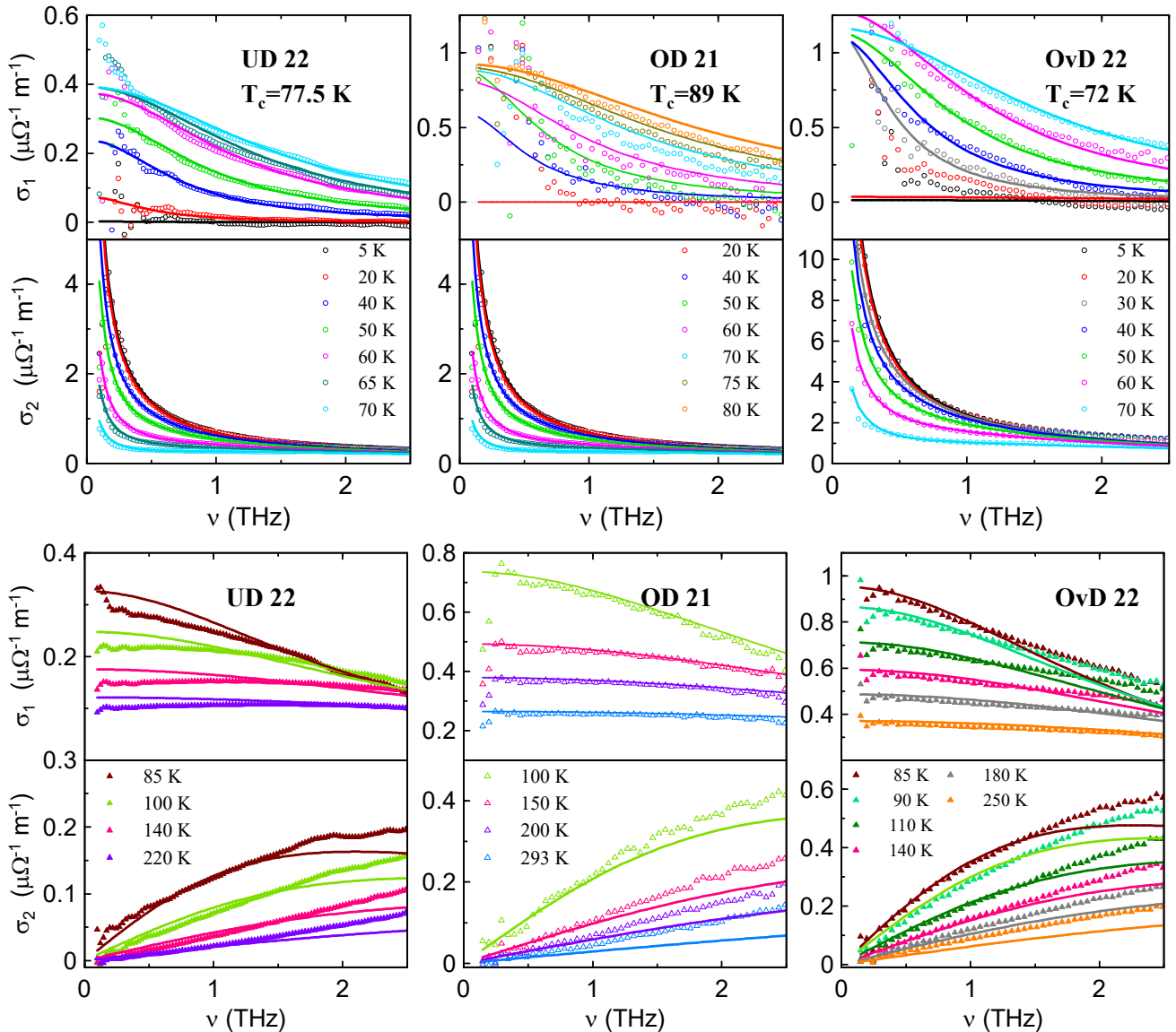


FIG. 3. Real and imaginary parts of the complex conductivity of underdoped UD22 (left), nearly optimally doped OD 21 (middle) and overdoped OvD22 (right) samples for  $T < T_c$  (top) and for  $T > T_c$  (bottom). Points - experimental data, curves - fit by the two-fluid model (eq. 1) for  $T < T_c$  and by Drude model for  $T > T_c$ .

case, the extracted thickness difference ( $d_{\text{ref}} - d_{\text{sub}}$ ) equals  $10.8 \mu\text{m}$ . This value is then used in further calculations.

#### IV. RESULTS AND DISCUSSION

Here, we present the terahertz conductivity up to 2.5 THz for three different dopings of  $\text{YBa}_2\text{Cu}_3\text{O}_{7-\delta}$  in Fig. 3 for the superconducting state (upper graphs) and for the normal state (bottom graphs): the optimally doped OD 21 (middle), the underdoped UD 22 (left) and the overdoped OvD 22 (right) cases. We underline that not all experimentally acquired data are shown in the graphs for clarity.

In the superconducting state, the two-fluid model describes the complex conductivity quite well for our dopings. In the fitting procedure, the quantity  $ne^2/m$  was assumed to be the same for all temperatures, not only for temperatures below  $T_c$ , and the values are listed in table II. On the other hand, the superfluid fraction  $f_s$  and the scattering rate  $1/\tau$  were fitted for each temperature independently. The imaginary part of the conductivity  $\sigma_2(\nu)$  is governed by a  $1/\nu$  behaviour and only at temperature near  $T_c$  or for  $\nu$  above 2 THz a non-negligible contribution from the normal fluid was observed. The real part  $\sigma_1$  is well described by the Drude response weighted by the normal fluid fraction  $(1 - f_s)$  except for all frequencies where  $\sigma_1$  is determined less reliably because of

the dominating  $\sigma_2$  term (for instance below 20 K). In the normal state,  $\sigma_1$  dominates over  $\sigma_2$  in contrast with the low-temperature limit below  $T_c$ . Thus  $\sigma_1$  is determined more reliably here. In optimally doped and overdoped cases, the Drude model describes the data both qualitatively and quantitatively reasonably well. However, for the underdoped sample, the experimental data starts to deviate from the Drude response, which is not surprising given the unusual properties of YBaCuO in the pseudogap regime. We speculate that for underdoped samples with lower  $T_c$  the discrepancy will even grow.

The scattering rate  $1/\tau$  was determined from the Drude model when below  $T_c$  the two-fluid model was used to account for the superfluid component and it is plotted for all cases, underdoped, optimally doped and overdoped samples (Fig. 4). All presented scattering rate collapse on each other below 100 K. At low temperatures, where the fraction of the normal state is almost zero, the determination of the scattering is no longer reliable. Above  $T_c$ , the scattering rate differs for each sample. For optimally doped and overdoped cases,  $1/\tau$  is well described by a linear dependence and in the graph it is even extrapolated below  $T_c$ . This is in agreement with the linear behaviour of the DC resistivity, see graph 1. However, the normal state of the underdoped sample shows a different behaviour as  $1/\tau$  is proportional to  $(T - T_c)^\beta$ , where we found the best agreement for  $\beta = (0.68 \pm 0.01)$ , which differs from the DC resistivity exponent which was found to be 0.34. One reason for this discrepancy might be that the behaviour of the underdoped sample starts to deviate from the Drude model thus the scattering rate is not reliably determined.

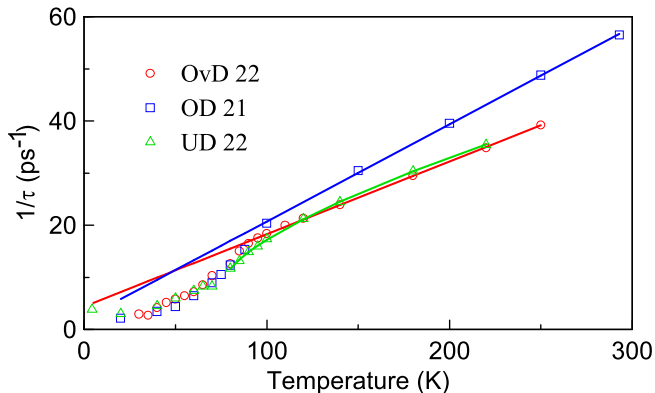


FIG. 4. Scattering rate  $1/\tau$  for underdoped UD22 (green triangles), optimally doped OD21 (blue squares) and overdoped OvD22 (red circles) samples. Solid curves corresponds to the fits described in detail in the text.

Let's now analyse the temperature dependence of the imaginary part of the conductivity  $\sigma_2$  and of the superconducting fluid fraction  $f_s$  which was determined from the fit by the two-fluid model.  $f_s(T)$  is usually written in the equal form of  $\lambda_0^2/\lambda(T)^2$  which can be shown using equations 2 and 3. At low temperatures, the London penetration depth  $\lambda$  appears to be temperature indepen-

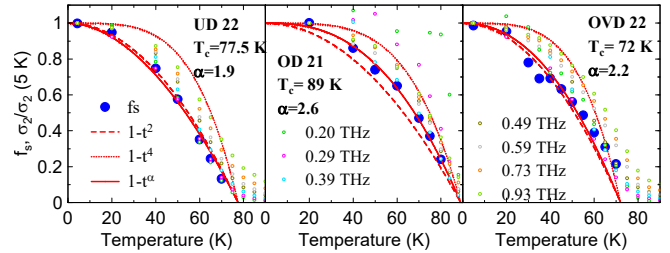


FIG. 5. Temperature dependence of the superfluid volume fraction of underdoped UD22 (left), nearly optimally doped OD 21 (middle) and overdoped OvD22 (right) samples. Large blue circle are determined from the two-fluid model, other points represent the ratio  $\sigma_2/\sigma_2(5K)$ .

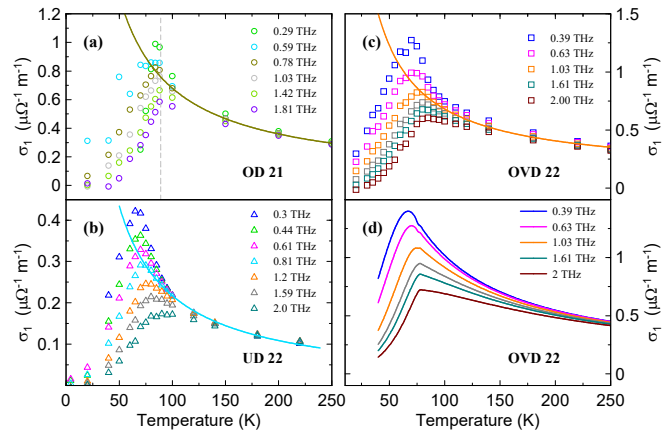


FIG. 6. Temperature dependence of the real part of the conductivity  $\sigma_1(T)$  for different frequencies for the three cases of doping: (a) nearly optimally doped OD21, (b) underdoped OD22 and (c) overdoped OvD22 samples. The peaks shift only marginally with the frequency. In the normal state, the conductivity is inversely proportional to temperature which is shown by solid line for one frequency in each case. (d) A reconstruction of the temperature dependence of the conductivity is shown for the optimally doped sample OvD 22.

dent, thus we use its value at 5 or 20 K as  $\lambda_0$ , see Table II. The London penetration depth  $\lambda$  can be extracted from the THz spectra in three various ways: (i) directly from  $\sigma_2$  using London formula 2, (ii) fitting  $\sigma_2(\omega)$  by a  $1/\omega$  law and (iii) fitting the complex conductivity by the two-fluid model. The results obtained by methods (i) and (iii) are compared in Fig. 5 for the optimally doped sam-

TABLE II. Parameters of the investigated samples.  $\lambda_0$  determined from  $\sigma_2$  at the lowest temperature

Sample	$\alpha$	$ne^2/m$	$\lambda_0(\text{nm})$
UD 22	1.9	$4.3 \times 10^{18}$	425
OD 1001 [13]	3.3	$1.4 \times 10^{19}$	240
OD 21	2.6	$1.5 \times 10^{19}$	230
OvD 22	2.2	$1.5 \times 10^{19}$	230

ple (middle), the underdoped sample (top) and the overdoped sample (bottom). All methods give qualitatively the same results. Method (i) seems to be reliable only for small frequencies, since for frequencies above 0.3 THz the values are frequency dependent and with increasing frequencies,  $\lambda$  is shifted towards higher values. This can be easily understood as an increase of the contribution of the normal fluid to the imaginary part  $\sigma_2$ , which is no longer negligible. Since only method (iii) separates the contribution of the normal and of the superfluid states, it is more reliable than other methods, provided the Drude model describes the normal fluid contribution correctly. This might not be the case for strongly underdoped samples.

The obtained values of the superfluid fraction  $f_s$  for several temperatures are compared with  $1 - (T/T_c)^2$  and Gorter-Casimir's  $1 - (T/T_c)^4$ . Furthermore,  $f_s(T)$  is fitted by equation 3 and we found out that it successfully describes the temperature dependence for all samples. The values of  $\alpha$  for all samples are listed in Table II. They are clustered around 2, corresponding to the quadratic dependence which is predicted for d-wave superconductors with strong impurity scattering. We did not observe the pronounced linear dependence which is predicted for the case of d-wave pairing, contrary to Bozovic's findings in  $\text{La}_{2-x}\text{Sr}_x\text{CuO}_4$  films in a broad range of oxygen doping [21].

We extracted the temperature dependence of the real part of the complex conductivity  $\sigma_1(T)$  at given frequencies from the spectra presented in Fig 3. A peak can be observed for each doping and its exact shape depends on the quality of the sample (Fig. 6). Similar coherence-like peaks in  $\sigma_1(T)$  were reported in previous studies in YBCO samples [2–5]. At low frequencies, the real part of the conductivity  $\sigma_1$  is determined less reliably due to the dominating  $1/\omega$  frequency dependence of the imaginary part  $\sigma_2$ , thus the data below 0.3 THz show some unphysical fluctuations. From room temperature down to the critical temperature,  $\sigma_1(T)$  grows following a  $1/T$  dependence of the scattering time. Below  $T_c$ ,  $\sigma_1$  steeply increases, reaches its maximum and decreases as the normal fluid fraction sharply falls. The peak position depends only slightly on the frequency. This frequency dependence suggests that it does not correspond to the

coherence peak predicted by the BCS theory, as it was discussed in Frenkel paper [6].

The analysis of the spectra suggests that this peak is the product of the competition between  $\tau(T)$  and  $f_s(T)$ . The scattering time and the normal fluid fraction, obtained from the fits in Fig. 4 and 5, were interpolated and these values were used in the equation 1 to reconstruct  $\sigma_1(T)$ . The model qualitatively and semi-quantitatively describes all the data for all frequencies (Fig. 6d).

## V. SUMMARY AND CONCLUSION

Using the two-fluid model, we analyzed the THz conductivity in the range of 0.2 to 2.5 THz for three qualitatively stoichiometries of YBaCuO: underdoped, optimally doped and overdoped samples. The two-fluid model successfully describes the response of all samples. Above the critical temperature, the Drude model describes the real part of conductivity  $\sigma_1(\nu)$  well but we observed some deviations in the underdoped sample. We studied the temperature dependence of the scattering rate  $1/\tau(T)$ , of the superfluid fraction  $f_s(T)$  and of the real part of conductivity  $\sigma_1(T)$ . The temperature dependences of scattering rate for studied samples differs above  $T_c$ , but they collapse on each other below 100 K. The superfluid volume fraction  $f_s(T)$  follows a quadratic temperature dependence which suggests a dirty d-wave superconductor case for all levels of doping. We found a coherence-like peak in  $\sigma_1(T)$  not only in underdoped and optimally doped samples, in agreement with previous studies [2–4, 6], but the same feature is also present in the overdoped sample. The coherence-like peak is the result of the competition of the temperature dependence of the scattering rate  $1/\tau(T)$  and the normal state fraction  $1 - f_s(T)$ .

## VI. ACKNOWLEDGMENT

We gratefully acknowledge helpful conversations with P. Lipavský. We acknowledge the financial support by the Czech Science Foundation (Project No. 21-11089S) and the National Science and Technology Council of Taiwan (Project No. 110-2119-M-A49-002-MBK)

- 
- [1] L. Taillefer, *Annu. Rev. Condens. Matter Phys.* **1**, 51 (2010).
  - [2] M. C. Nuss, P. M. Mankiewich, M. L. O'Malley, E. H. Westerwick, and P. B. Littlewood, *Phys. Rev. Lett.* **66**, 3305 (1991).
  - [3] C. Ludwig, Q. Jiang, J. Kuhl, and J. Zegenhagen, *Phys. C: Supercond.* **269**, 249 (1996).
  - [4] A. Pimenov, A. Loidl, G. Jakob, and H. Adrian, *Phys. Rev. B* **59**, 4390 (1999).
  - [5] A. Pimenov, A. Loidl, G. Jakob, and H. Adrian, *Phys. Rev. B* **61**, 7039 (2000).
  - [6] A. Frenkel, F. Gao, Y. Liu, J. F. Whitaker, C. Uher, S. Y. Hou, and J. M. Phillips, *Phys. Rev. B* **54**, 1355 (1996).
  - [7] J. Bardeen, L. N. Cooper, and J. R. Schrieffer, *Phys. Rev.* **106**, 162 (1957).
  - [8] J. Annett, N. Goldenfeld, and S. R. Renn, *Phys. Rev. B* **43**, 2778 (1991).
  - [9] M. Prohammer and J. P. Carbotte, *Phys. Rev. B* **43**, 5370 (1991).

- [10] C. J. Gorter and H. G. B. Casimir, *Z. Phys.* **35**, 963 (1934).
- [11] S. D. Brorson, R. Buhleier, I. E. Trofimov, J. O. White, C. Ludwig, F. F. Balakirev, H.-U. Habermeier, and J. Kuhl, *J. Opt. Soc. Am. B* **13**, 1979 (1996).
- [12] S.-W. Huang, L. A. Wray, Y.-C. Shao, C.-Y. Wu, S.-H. Wang, J.-M. Lee, Y.-J. Chen, R. W. Schoenlein, C. Y. Mou, Y.-D. Chuang, and J.-Y. Lin, *Phys. Rev. B* **107**, 134513 (2023).
- [13] R. Tesař, M. Šindler, C. Kadlec, P. Lipavský, L. Skrbek, and J. Kolářček, *Sci. Rep.* **11** (2021).
- [14] Y.-J. Chen, M. G. Jiang, C. W. Luo, J.-Y. Lin, K. H. Wu, J. M. Lee, J. M. Chen, Y. K. Kuo, J. Y. Juang, and C.-Y. Mou, *Phys. Rev. B* **88**, 134525 (2013).
- [15] C. Luo, C. C. Lee, C. H. Li, H. C. Shih, Y.-J. Chen, C. C. Hsieh, C. H. Su, W. Y. Tzeng, K. H. Wu, J. Y. Juang, T. M. Uen, S. P. Chen, J.-Y. Lin, and T. Kobayashi, *Opt. Express* **16**, 20610 (2008).
- [16] C. W. Luo, M. H. Chen, S. P. Chen, K. H. Wu, J. Y. Juang, J.-Y. Lin, T. M. Uen, and Y. S. Gou, *Phys. Rev. B* **68**, 220508 (2003).
- [17] M. Presland, J. Tallon, R. Buckley, R. Liu, and N. Flower, *Phys. C: Supercond.* **176**, 95 (1991).
- [18] R. Liang, D. A. Bonn, and W. N. Hardy, *Phys. Rev. B* **73**, 180505 (2006).
- [19] A. Nahata, A. S. Weling, and T. F. Heinz, *Appl. Phys. Lett.* **69**, 2321 (1996).
- [20] We are using the convention  $E(t) = E_0 \exp(-i\omega t)$  which implies the following forms of the complex quantities: conductivity  $\tilde{\sigma} = \sigma_1 + i\sigma_2$ , permittivity  $\tilde{\varepsilon} = \varepsilon_1 + i\varepsilon_2$ , and refractive index  $\tilde{n} = n + i\kappa$ .
- [21] I. Božović, A. T. Bollinger, J. Wu, and X. He, *Low Temp. Phys.* **44**, 519 (2018).